Available online at www.sciencedirect.com
SCIENCE DIRECT®

Applied Mathematical Modelling 30 (2006) 1326–1342

APPLIED MATHEMATICAL MODELLING

www.elsevier.com/locate/apm

Numerical study of gas–solid flow in a cyclone separator

B. Wang [a,b], D.L. Xu [b], K.W. Chu [a], A.B. Yu [a,*]

[a] *Center for Simulation and Modelling of Particulate Systems and School of Materials Science and Engineering, University of New South Wales, Sydney, NSW 2052, Australia*

[b] *Institute of Powder Engineering, School of Materials Science and Engineering, Xi'an University of Architecture and Technology, Xi'an 710055, PR China*

Received 14 July 2004; accepted 19 September 2005
Available online 24 April 2006

Abstract

This paper presents a numerical study of the gas–powder flow in a typical Lapple cyclone. The turbulence of gas flow is obtained by the use of the Reynolds stress model. The resulting pressure and flow fields are verified by comparing with those measured and then used in the determination of powder flow that is simulated by the use of a stochastic Lagrangian model. The separation efficiency and trajectory of particles from simulation are shown to be comparable to those observed experimentally. The effects of particle size and gas velocity on separation efficiency are quantified and the results agree well with experiments. Some factors which affect the performance of cyclone were identified. It is shown that the collision between gas streams after running about a circle and that just entering occurred around the junction of the inlet duct and the cylinder of the cyclone, resulting in a short-circuiting flow. The combination of flow source and sink was distributed near the axis of cyclone, forming a flow dipole at axial section. Particles entering at different positions gave different separation efficiency. A particle with size exceeding a critical diameter, which was condition-dependant, would stagnate on the wall of cyclone cone. This was regarded as one of the main reasons for the deposition on the inner conical surface in such cyclones used in the cement industry.

Keywords: Cyclone; Gas-particle flow; Computational fluid dynamics; Stochastic Lagrangian model

1. Introduction

Gas cyclone separator is widely used in industries to separate dust from gas or for product recovery because of its geometrical simplicity, relative economy in power and flexibility. The conventional method of predicting the flow field and the collection efficiency of a cyclone is empirical. In the past decade, application of computational fluid dynamics (CFD) for the numerical calculation of the gas flow field becomes more and more popular. One of the first CFD simulations was done by Boysan [1]. He found that the standard k–ε turbulence model is inadequate to simulate flows with swirl because it leads to excessive turbulence viscosities and

* Corresponding author. Tel.: +61 2 9385 4429; fax: +61 2 9385 5956.
E-mail address: a.yu@unsw.edu.au (A.B. Yu).

0307-904X/$ - see front matter
doi:10.1016/j.apm.2006.03.011

Nomenclature

C_D	drag coefficient
d	particle diameter, m
$\bar{d}$	characteristic diameter
F_k	momentum transport coefficient, t^{-1}
g	acceleration due to gravity, m s^{-2}
m	particle mass, kg
n	distribution parameter
p'	dispersion pressure, Pa
r_p	radius of particle, m
Re	Reynolds number
t	time, s
u	instantaneous velocity, m s^{-1}
u'	dispersion velocity, m s^{-1}
$\bar{u}$	time average velocity in axial direction, m s^{-1}
u_p	particle instantaneous velocity in axial direction, m s^{-1}
v_p	particle instantaneous velocity in radial direction, m s^{-1}
$\bar{v}$	time average velocity in radial direction, m s^{-1}
w_p	particle instantaneous velocity in tangential direction, m s^{-1}
$\bar{w}$	time average velocity in tangential direction, m s^{-1}
x	axis, m
δ	Kronecker factor
μ	fluid viscosity, kg m^{-1} s^{-1}
ρ	density, kg m^{-3}

Subscripts

g	gas
i,j,k	1, 2, 3
p	particle
t	tangential direction
z	axial direction

unrealistic tangential velocities. Recent studies suggest that Reynolds stress model (RSM) [2–4] can improve the accuracy of numerical solution.

Currently, particle turbulent dispersion due to interaction between particles and turbulent eddies of fluid is generally dealt with by two methods [5]: mean diffusion which characterizes only the overall mean (time-averaged) dispersion of particles caused by the mean statistical properties of the turbulence, and structural dispersion which includes the detail of the non-uniform particle concentration structures generated by local instantaneous features of the flow, primarily caused by the spatial-temporal turbulent eddies and their evolution. To predict the mean particle diffusion in turbulent flow, both Lagrangian and Eulerian techniques can be used. Since the early work of Yuu et al. [6] and Gosman and Ioannides [7], the stochastic Lagrangian model has shown significant success in describing the turbulent diffusion of particles. It has been reported that it is necessary to trace up to 3×10^5 particle trajectories in order to achieve statistically meaningful solution even for a two-dimensional flow [8,9]. In order to enhance such application in industries, some modified models were proposed. Sommefeld and Simonin [10] proposed Langevin stochastic differential equation models by making use of possibility density function (PDF). Litchford and Jeng [11] developed a stochastic dispersion-width transport model, where the dispersion-width is explicitly computed through the linearized equation of motion using the concept of particle–eddy interactions. Moreover, Chen and Pereira [12] reported a SPEED model where a combined stochastic-probabilistic method is used to

describe the turbulent motion of discrete particles so that only a small number of particle trajectories are required.

In this paper, we used the RSM and stochastic Lagrangian model in the commercial software package "Fluent" to study the gas–solid flow in a typical Lapple cyclone separator. The model is verified by comparing the simulated and measured results in term of gas pressure and flow field, solid flow pattern and collection efficiency. The effects of particle size, gas velocity and inlet condition are investigated.

2. Model description

There are three models commonly used in cyclone simulation: k–ε model, algebraic stress model (ASM) and RSM. The k–ε model adopts the assumption of isotropic turbulence, so it is not suitable for the flow in a cyclone which has anisotropic turbulence. ASM cannot predict the recirculation zone and Rankine vortex in strongly swirling flow [13]. RSM forgoes the assumption of isotropic turbulence and solves a transport equation for each component of the Reynolds stress. It is regarded as the most applicable turbulent model for cyclone flow even though it has the disadvantage of being computationally more expensive [2–4].

In the RSM, the transport equation is written as

$$\frac{\partial}{\partial t}(\rho\overline{u_i'u_j'}) + \frac{\partial}{\partial x_k}(\rho u_k\overline{u_i'u_j'}) = D_{ij} + P_{ij} + \Pi_{ij} + \varepsilon_{ij} + S, \tag{1}$$

where the left two terms are the local time derivative of stress and convective transport term, respectively. The right five terms are

the stress diffusion term: $$D_{ij} = -\frac{\partial}{\partial x_k}\left[\rho\overline{u_i'u_j'u_k'} + \overline{(p'u_j')}\delta_{ik} + \overline{(p'u_i')}\delta_{jk} - \mu\left(\frac{\partial}{\partial x_k}\overline{u_i'u_j'}\right)\right],$$

the shear production term: $$P_{ij} = -\rho\left[\overline{u_i'u_k'}\frac{\partial u_j}{\partial x_k} + \overline{u_j'u_k'}\frac{\partial u_i}{\partial x_k}\right],$$

the pressure-strain term: $$\Pi_{ij} = \overline{p\left(\frac{\partial u_i'}{\partial x_j} + \frac{\partial u_j'}{\partial x_i}\right)},$$

the dissipation term: $$\varepsilon_{ij} = -2\mu\overline{\frac{\partial u_i'}{\partial x_k}\frac{\partial u_j'}{\partial x_k}},$$

and the source term: S.

In the modelling of particle dispersion, the interaction between particles is neglected since only dilute flow is considered in this work. Only the gravity and gas drag forces on particles are calculated. Gas drag force is decomposed into two components: one caused by average velocity of fluid, and another caused by the dispersion velocity of fluid. Then the momentum equation of a particle in the two-phase flow at ambient temperature can be expressed as

$$\frac{\mathrm{d}u_\mathrm{p}}{\mathrm{d}t} = F_k(\bar{u} + u' - u_\mathrm{p}) - g, \tag{2}$$

$$\frac{\mathrm{d}v_\mathrm{p}}{\mathrm{d}t} = F_k(\bar{v} + v' - v_k) + \frac{w_\mathrm{p}^2}{r_\mathrm{p}}, \tag{3}$$

$$\frac{\mathrm{d}w_\mathrm{p}}{\mathrm{d}t} = F_k(\bar{w} + w' - w_\mathrm{p}) - \frac{v_\mathrm{p}w_\mathrm{p}}{r_\mathrm{p}}, \tag{4}$$

where $F_k = \frac{18\mu}{d_\mathrm{p}^2\rho_\mathrm{p}}C_\mathrm{D}\frac{Re_\mathrm{p}}{24}$ is the momentum transport coefficient between fluid and particles, and the drag coefficient is given as

$$C_\mathrm{D} = \begin{cases} \dfrac{24}{Re} & Re_\mathrm{p} \leqslant 1, \\ \dfrac{24(1 + 0.15Re_\mathrm{p}^{0.687})}{Re_\mathrm{p}} & 1 < Re_\mathrm{p} \leqslant 1000, \\ 0.44 & Re_\mathrm{p} > 1000, \end{cases}$$

where $Re_p = \frac{d_p \rho_g |\vec{\varphi}_g - \vec{\varphi}_p|}{\mu}$ is the particle Reynolds number, φ can be u, v and w. When the particle interacts with fluid eddy, u', v', w' is obtained by sampling from an isotropic Gaussian distribution with a standard deviation of $\sqrt{2k/3}$. Particle–eddy interaction time and dimension should not be larger than the lifetime and size of a random eddy.

3. Condition for numerical and physical experiments

The cyclone considered is a typical Lapple cyclone. Fig. 1(a) shows the notations of the cyclone dimensions and Table 1 gives their values. Fig. 1(b) shows the computational domain, containing 45,750 CFD cells. The whole computational domain is divided by structured hexahedron grids. At the zone near wall and vortex finder the grids are dense, while at the zone away from wall the grids are refined. Three grid domains were tested in our preliminary computation, containing 25,900, 47,750, 95,350 cells, respectively. The difference is less than 5% for all variables examined, suggesting that computed results are independent of the characteristics of the mesh size.

Physical experiments have also been conducted to validate the numerical model. In such an experiment, air was blown into the inlet of the cyclone, with its flowrate measured by a flowmeter. The inlet gas velocity and the particle velocity were both 20 m/s. The exit tube was open to the air and the gas pressure at the top of the vortex finder was 1 atm. The volume fraction of particle phase was less than 10%.

A five-hole probe consisting of an adjustable frame and five pressure transducers was used to measure the velocity and pressure of the gas field. When the five-hole probe was placed in a flow field, voltage signals obtained through the five pressure transducers were transferred to an amplifier. The magnified voltage signals were acquired through a data acquisition system containing a microprocessor and a personal computer.

The material used was a typical cement raw material. Its particle size distribution can be well described by the Rosin–Rammler equation:

$$R(d) = \exp\lfloor -(d/\bar{d})^n \rfloor, \tag{5}$$

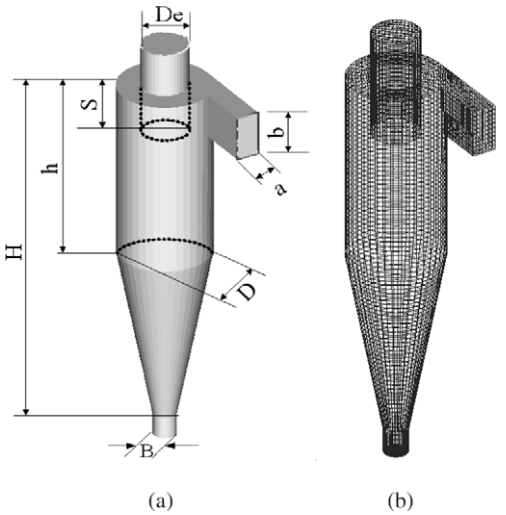

Fig. 1. Schematic and grid representation of the cyclone considered.

Table 1
Geometry of the cyclone considered ($D = 0.2$ m)

a/D	b/D	De/D	S/D	h/D	H/D	B/D
0.25	0.5	0.5	0.625	2.0	4.0	0.25

where d is particle diameter, and $R(d)$ means the mass fraction of droplets with diameter greater than d. The characteristic diameter $\bar{d}$ equals 29.90 μm and the distribution parameter n is 0.806. The particle density is 3320 kg/m^3.

4. Results and discussion

4.1. Gas flow field

4.1.1. Pressure field

Fig. 2 shows that the static pressure decreases radially from wall to centre, and a negative pressure zone appears in the centre. The black line in Fig. 2(A–A) is the dividing line between the positive static pressure and negative static pressure. The pressure gradient is the largest along radial direction, as there is a highly intensified forced vortex.

Fig. 3 shows the relationship between the pressure drop and the inlet gas velocity. With the increase of the inlet gas velocity, the pressure drop increases. The experimental data obtained agree reasonably well with the calculated results, although they are consistently slightly higher.

4.1.2. Tangential velocity

Fig. 4 shows the experimental and calculated tangential velocities at the cylindrical section of the cyclone. The simulation results are in good agreement with the experimental results. The flow field in the cyclone indicates the expected forced/free combination of the Rankine type vortex. Moreover, because the cyclone has only one gas inlet, the axis of the vortex does not coincide with the axis of the geometry of cyclone.

Fig. 5 shows the calculated tangential velocity distribution in detail. The tangential velocity distribution is similar to the dynamic pressure distribution. This means the tangential velocity is the dominant velocity in the cyclone. The value of the tangential velocity equals zero on the wall and in the centre of the flow field. From Fig. 5(C–C), it can be seen that high speed gas enters the inlet and is accelerated up to 1.5–2.0 times of the inlet velocity at point A. Then the velocity decreases as the gas spins down along the wall. Before it goes below the vortex finder, the gas flow collides with the follow-up flow and forms a chaotic flow close to the vortex finder outside wall (point B). In the meantime, gas velocity decreases sharply at point B, and may even be in the reverse direction. It would increase the loss of energy and the pressure drop in cyclone. This is the main cause

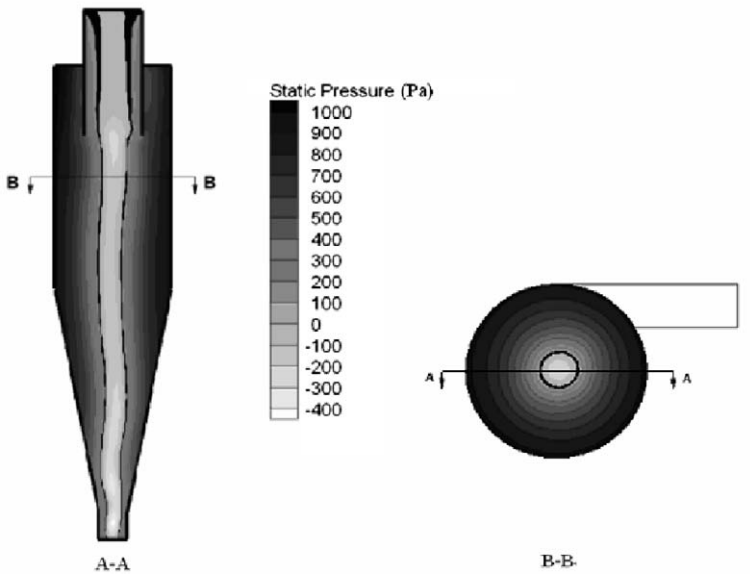

Fig. 2. Contour of static pressure with the zero pressure highlighted by the line in section A–A.

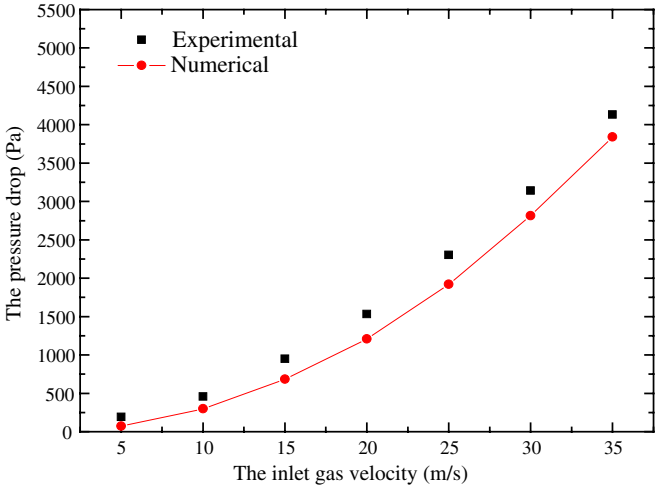

Fig. 3. Experimental vs. calculated pressure drops.

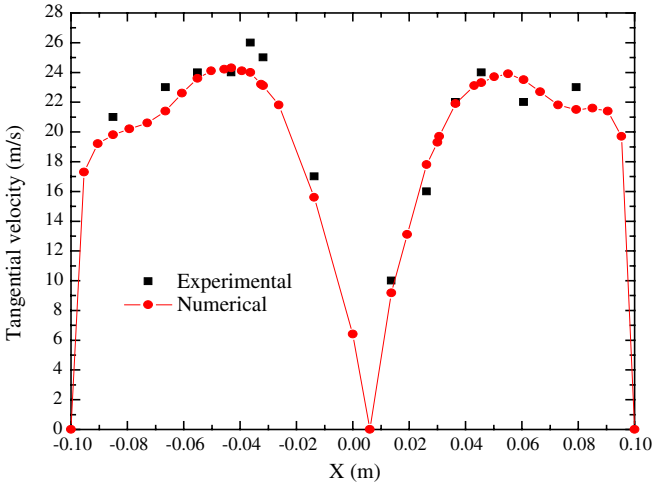

Fig. 4. Experimental vs. calculated tangential velocities.

of the short-circuiting flow and often results in a high pressure drop. To overcome this problem, it is suggested that the inlet shape should be modified [14].

4.1.3. Axial velocity

Fig. 6 shows that the forced vortex is a helical twisted cylinder and not completely axially symmetric, especially in the conical part. The results are qualitatively similar to those obtained by Cullivan et al. [15] for hydrocyclone. The black line in Fig. 6(A–A) is the dividing line between the upward flow and the downward flow. The diameter of upward flow is slightly larger than that of the vortex finder. Moreover, since much gas flows over into the vortex finder, the axial velocity reaches a peak value under the vortex finder. Meanwhile, the dip in axial velocity near the axis except the section under the vortex finder is clearly visible. It can be observed from Fig. 6(B–B) that the centre of the upward flow does not coincide with the geometrical centre of the cyclone. This should be one of the main reasons why there is an eccentric vortex finder in some cyclones to reduce the pressure drop. Fig. 5(C–C) also suggests that the presence of the eccentric vortex finder will help weaken the chaotic flow.

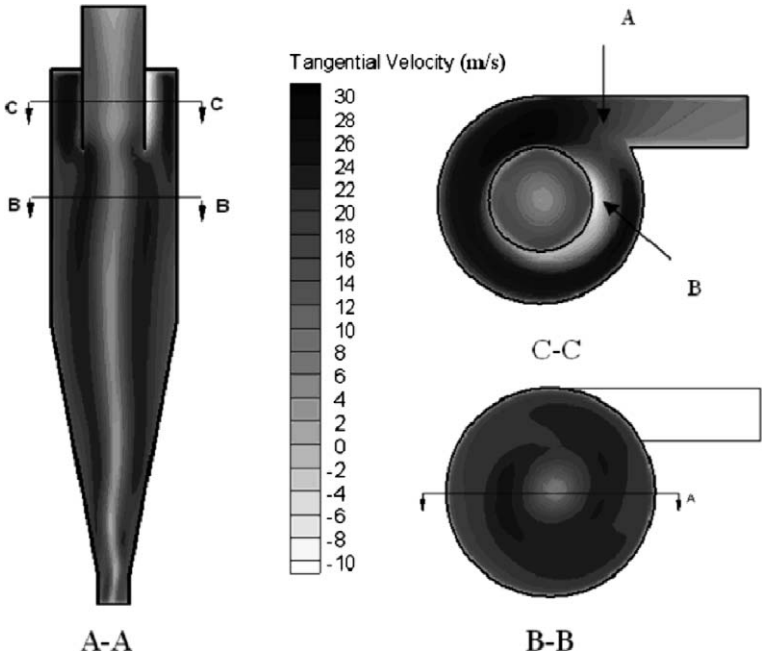

Fig. 5. Contour of tangential velocity (anti-clockwise is positive and clockwise is negative).

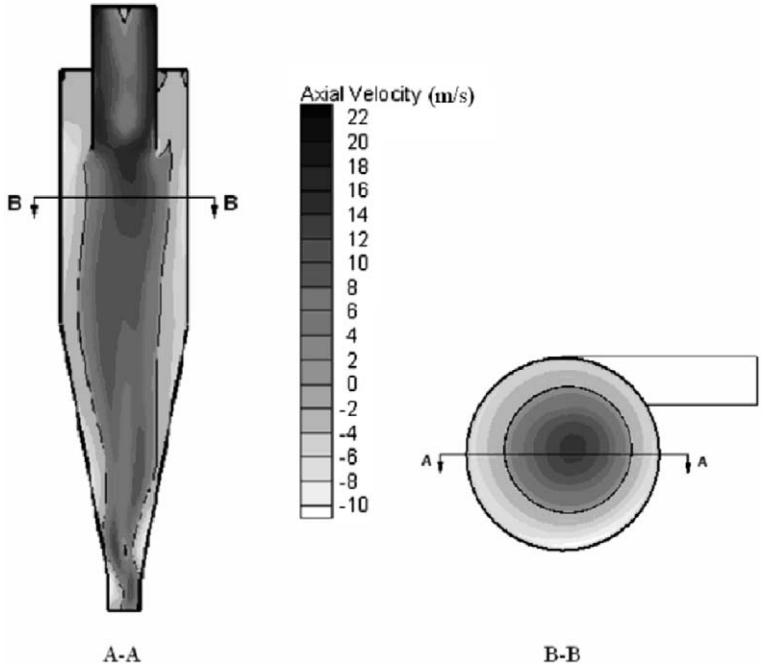

Fig. 6. Contour of axial velocity (upward is positive and downward is negative, the axial velocity on the line in section A–A equals zero).

4.1.4. Radial velocity

Fig. 7(A–A) shows that the forced vortex in the centre is a helical twisted cylinder. The axis of the forced vortex does not coincide with the geometrical axis of cyclone, and is not straight but curved. The distribution of radial velocity in the central vortex core based on the axially symmetric line is eccentric. The value of one

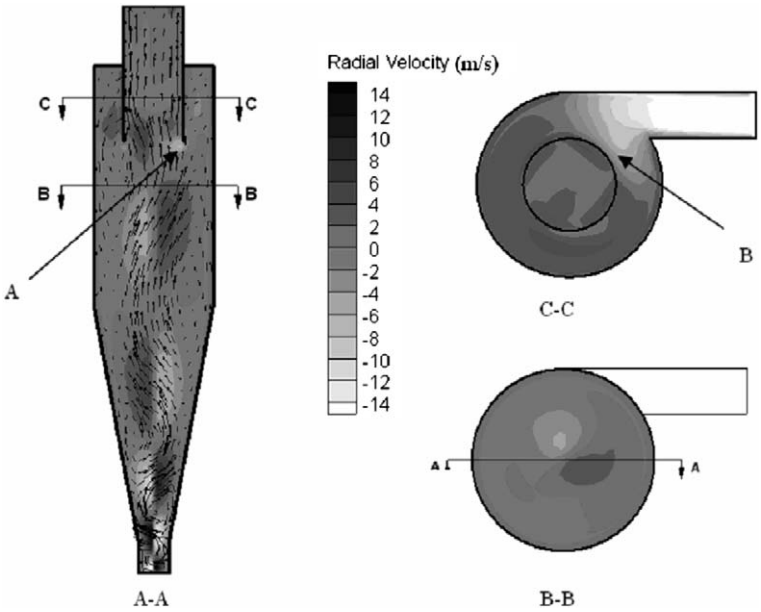

Fig. 7. Contour of radial velocity distribution (outward is positive and inward is negative).

side is positive and the other is negative. Thereby, the combination of flow source and sink is distributed near the axis of cyclone, forming a flow dipole at axial section, shown in Fig. 7(B–B). The orientation of dipole is observed to locate upward along the cyclone central line. This is probably mainly because the vortex rotates together with the flow around the geometric axis of the cyclone and has a pronounced helical structure [16]. This structure could be caused by the extrusion among gas, represented by the velocity vector in the figure, would result in instability in cyclone. There is a zone right under the vortex finder, at point A, where gas directly flows into the vortex finder instead of spinning down to the conical part and then flowing upward. Moreover, at point B, the radial velocity becomes negative again, directing to the centre, because of the collision among gas. Both points A and B indicate the short-circuiting flow, which deteriorates cyclone performance. In the conical part, the radial velocity is much larger than that of cylindrical part. Fig. 7(B–B) shows that the distribution of radial velocity is nearly uniform in the quasi-free vortex area. The distribution of the radial velocity in the forced vortex is eccentric because of the non-symmetrical geometry of the cyclone. Fig. 7(C–C) shows that the radial velocity is negative, corresponding to the inward flow in the gas inlet, and then becomes zero rapidly. Afterwards it becomes positive due to the effect of centrifugal force around the vortex finder.

4.1.5. Secondary circulation in cyclone

Secondary circulation can deteriorate the performance of cyclone. There are three regions where the secondary circulation formed by axial velocity and radial velocity occurs, as shown at points A, B and C in Fig. 8, respectively. Firstly, at point A, because of the collision among gas, part of gas flows inward and exhausts out quickly from the region right under the vortex finder, which forms a short-circuiting flow (it is also shown in Sections 4.1.2 and 4.1.4). Secondly, at point B, there is a slow laminar flow layer below the roof of the cyclone where the gas flows to and hits the roof, and flows reversely toward the vortex finder since the pressure reaches a lower value than in the strong rotational flow. This phenomenon is called the eddy flow. It can result in particles accumulating on the wall escaped from the vortex finder to the top, forming swilling dust ceiling, and decreasing the efficiency of separation. Thirdly, at point C, because of the enlarging dust box and the friction from particles accumulating walls, the rotational velocity of gas entering the dust box will decrease. Then the gas will turn back on the central line from dust box to cyclone body and mix with the following-up downward rotational flow, which causes intensive momentum transfer and energy loss. It is called eccentric circumfluence. The damage of short-circuiting flow (A) and eddy flow (B) can be reduced

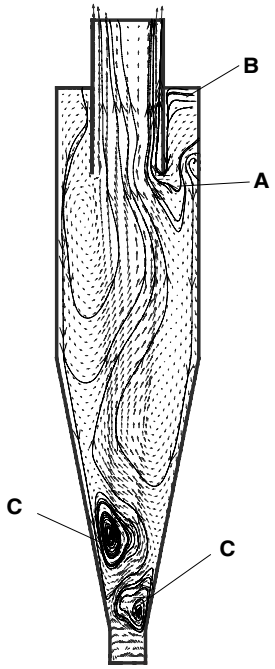

Fig. 8. Secondary circulation in cyclone.

by increasing the length of vortex finder in cyclone body. However, a longer vortex finder will result in a higher pressure drop in cyclone.

4.1.6. Comparison with other literature results

In order to validate the proposed model more generally, comparison has been extended to the Hoeksta's experiment [17] using a Stairmand high-efficiency cyclone. Fig. 9 shows the comparison between the numerical and experimental velocity profiles at three axial locations. The agreement between the simulated and experimental results is very good. In particular, details such as the asymmetry of the axial velocity profiles in the conical part of the cyclone are well reproduced by the model.

Recently, Schmidt et al. [18] reported that the exit tube length affects the overall flow properties of cyclones. To test if there is such an effect in the considered system, numerical computation has also been performed with different outflow lengths ranging from 0 to 4D. The results in Fig. 10 show the outflow length does not affect the flow field under steady state flow conditions. Unsteady state conditions may affect the flow field. However, this effect is not so significant. As shown in Fig. 11, the axial velocity profiles in cyclones with different outflow length are qualitatively comparable. Quantitatively, as shown in Fig. 12, changing the outflow length makes the data more scattered, but the pattern in tangential and axial velocity profiles is still maintained. Therefore, although seemingly short, a constant outflow length is used in this work, i.e. 0.5D. This value is also used in our physical experiment.

4.2. Particles flow pattern

4.2.1. The effect of inlet condition on separation efficiency

The separation efficiency for particles entering the cyclone at different position varies because they have different flow paths. Based on the computed results, it is found that the inlet area can be divided into four regions to describe this behaviour, as shown in Fig. 13. Fig. 14 shows the trajectories of particles with cut diameter $d_{c50} = 3 \times 10^{-7}$ m from the four different areas. The particle from region A escapes from vortex finder directly because of the short-circuiting flow mentioned above. The particle from region B has circular motion below the roof and may form swirling dust ceiling. Once it enters the central vortex, they cannot be collected.

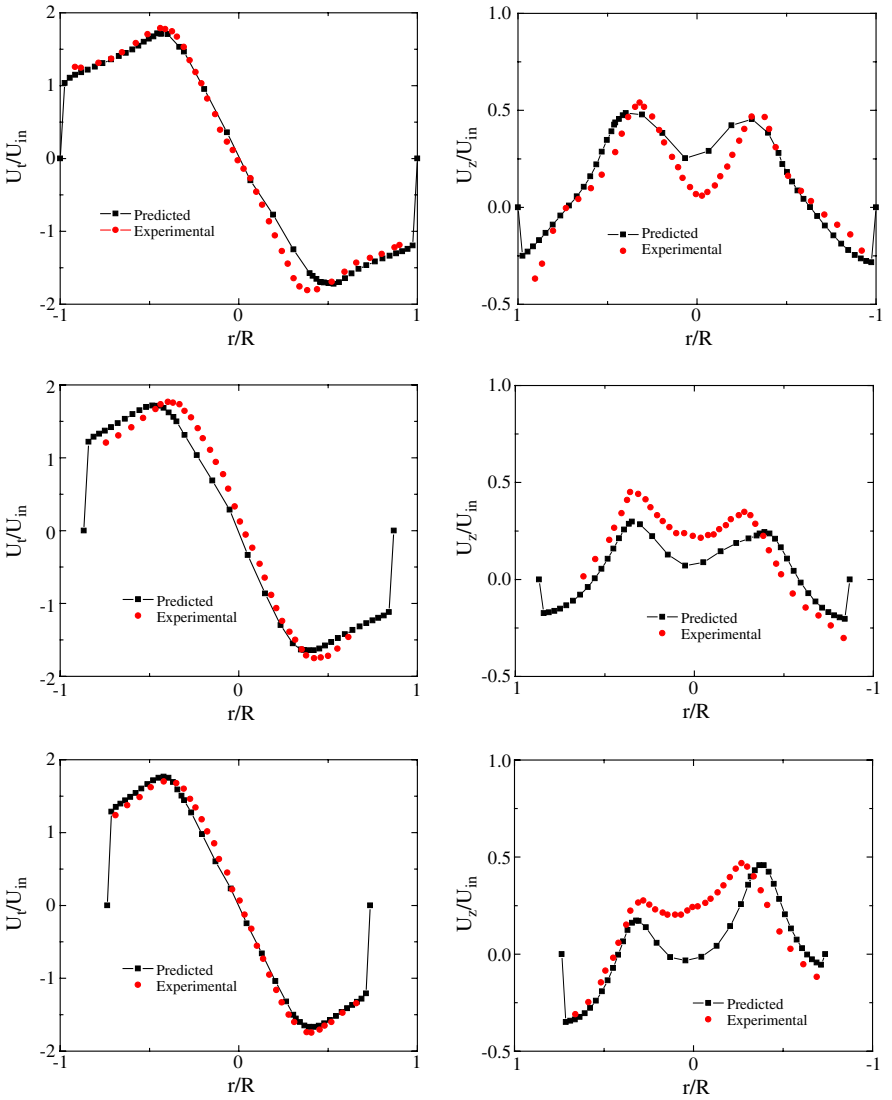

Fig. 9. Velocity profiles along the axis of the cyclone at three axial locations (from top to bottom: $z = 3.25D$, $z = 2.0D$ and $z = 1.5D$. The left is tangential velocity profile; the right is axial velocity profile).

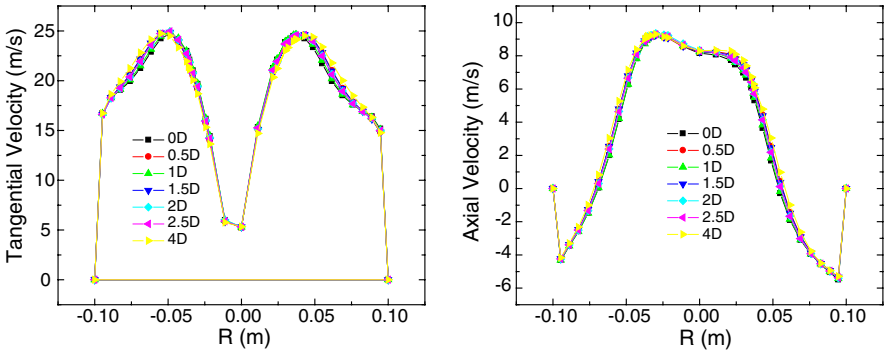

Fig. 10. The velocity profiles of cyclone with different outflow length under steady state conditions (left: tangential velocity, right: axial velocity).

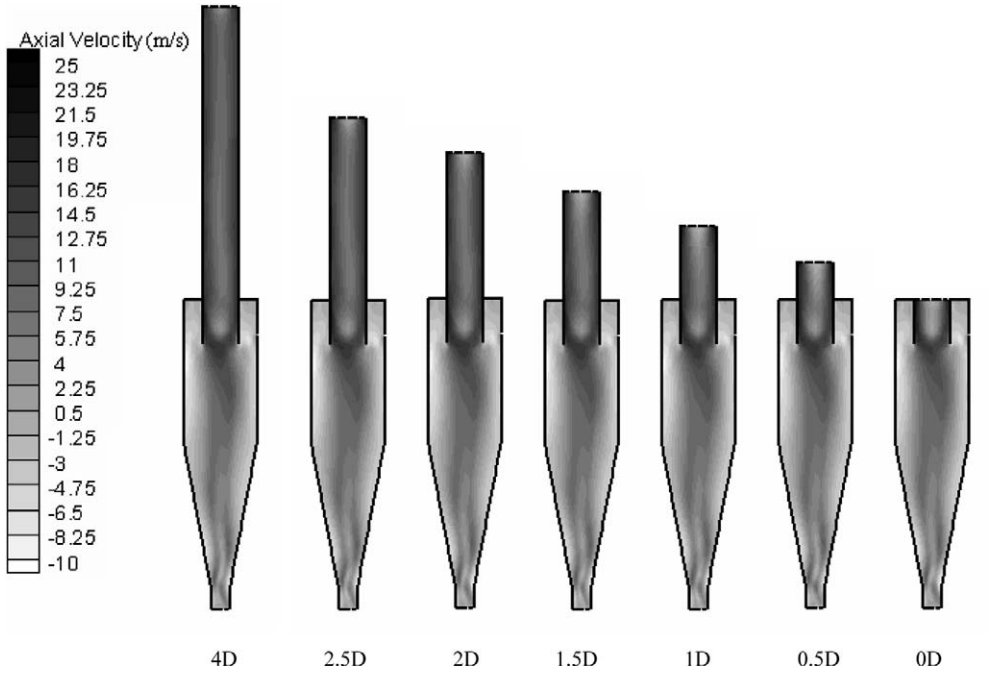

Fig. 11. Contour of axial velocity distributions with different outflow length under unsteady state conditions.

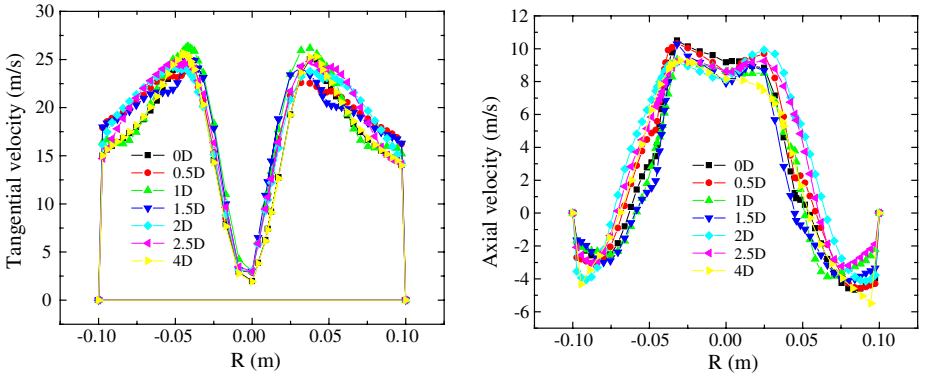

Fig. 12. The velocity profiles of cyclone with different outflow length under unsteady state conditions (left: tangential velocity, right: axial velocity, unsteady).

Particles from regions C and D collide with the wall, and go downwards to the separating space in the cyclone. The difference between particles from regions C and D is that particles from the latter take a shorter time to contact the wall.

Fig. 15 shows the experimental trajectories of particles entering from different inlet regions. Obviously, particles can have different descending angles. Particles entering from region A have high positions in the cylindrical part and their descending angle is small. In other words, if particles enter the cyclone from region A, the separation efficiency would be low. Entering from region B gives similar results, and the only difference is that particles from region B have lower positions, producing a higher separation efficiency. A particle entering from region C has a low position and its descending angle is big, meaning the separation efficiency is high. When particles enter from region D, the separation efficiency is the highest because they have a largest descending angle.

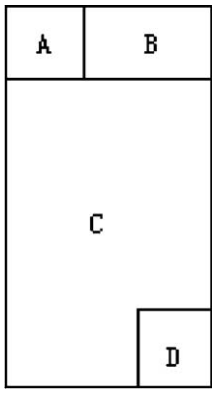

Fig. 13. Inlet area divided into four regions in this work.

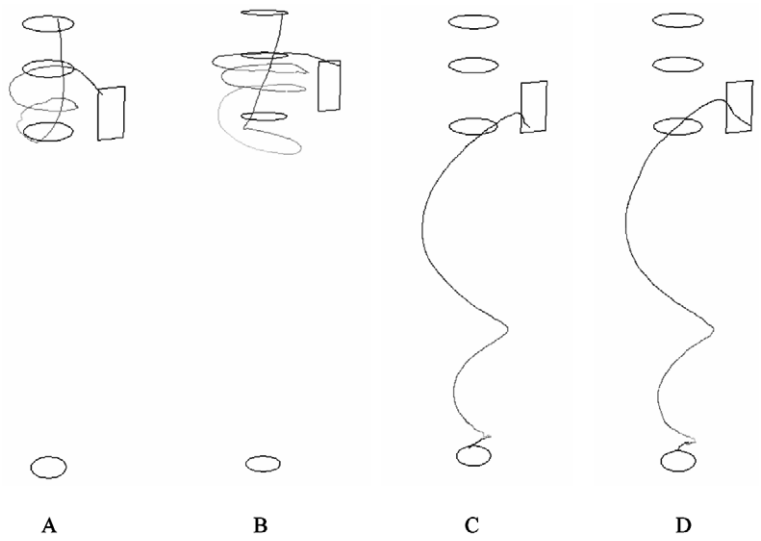

Fig. 14. The trajectories of particles with cut diameter $d_{c50} = 3 \times 10^{-7}$ m from different inlet regions (refer to Fig. 13).

Therefore, physical and numerical experiments produce results qualitatively comparable. In general, if particles enter the cyclone from the top part of the inlet, their separation efficiency will be relatively low. On the contrary, if particles enter the cyclone from the bottom of the inlet, their separation efficiency will be high. This factor should be taken into account in cyclone design and performance control, although more detailed studies are necessary to fully understand and quantify its effect.

4.2.2. The effect of particle diameter on residence time

Fig. 16 shows the change in location with time for 15,000 particles with five diameters within 1 s. It can be seen from this figure that the trajectory of the largest particles (red) concentrates in the upside of the cone, and the trajectory of the smallest particles (blue) is in the downside of the cone. The other three sized particles are largely in-between the two extremes.

As shown in Fig. 17, large particles are collected while small particles escape from the cyclone. Particles with a too small diameter cannot move outward to the wall of cyclone since the centrifugal force on them are not bigger than the gas drag force on particles. For the system considered in this work, particles with diameter of 2×10^{-6} m and 7×10^{-6} m can spin down to the conical part and then be collected while bigger

Fig. 15. Experimental results showing the trajectories of tracing particles entering from different inlet regions (refer to Fig. 13).

particles with diameter of 3×10^{-5} m and 1×10^{-4} m spin downward first and then keep spinning near the wall at a certain horizontal level.

In order to verify this numerical observation, physical experiments have been done by use of ceramic balls whose density is similar to the cement raw material. The experimental results are shown in Fig. 18. In Fig. 18(a), the original cement raw material was used. It was observed that particles flow downward at the cone section and display a certain descending angle. On the other hand, as shown in Fig. 18(b), large ceramic balls keep spinning at a certain height and do not show a descending angle. It indicates that the ceramic balls are difficult to be collected directly at the bottom. The result supports the numerical result. Interestingly, Bradley [19] reported a similar observation for hydrocyclone flow.

According to Fig. 17, particles with diameter of 2×10^{-6} m and 7×10^{-6} m can spin down to the conical part of cyclone and be collected at the bottom, while particles with diameter of 3×10^{-5} m and 1×10^{-4} m spin downward first and then keep spinning near the wall at a certain height. This is probably because when a big particle moves down to the conical body, the radius at the cyclone decreases, but the tangential velocity of the particle dose not change much. So the centrifugal force on the particle increases. Correspondingly, as shown in Fig. 19, the supporting force N increases, and the axial component force N_z increases too. When N_z is larger than the sum of gravity G and the axial component F_{Dz} of gas drag force, the particle moves up. If N_z is equal to the sum of the gravity and the axial component F_{Dz} of gas drag force, the particle will keep spinning at a certain height.

When a particle keeps spinning in the conical body, forces acting on the particle can be written as

$$G + F_{Dz} = N_z \tag{6a}$$

or

$$mg + 3\pi\mu d_p(u_{gz} - u_{pz}) = m\frac{u_{pt}^2}{r}tg\theta. \tag{6b}$$

Re-arranging the equation gives

$$g + \frac{18\mu}{d_p^2\rho_g}(u_{gz} - v_{pz}) = \frac{u_{pt}^2}{r}tg\theta. \tag{7}$$

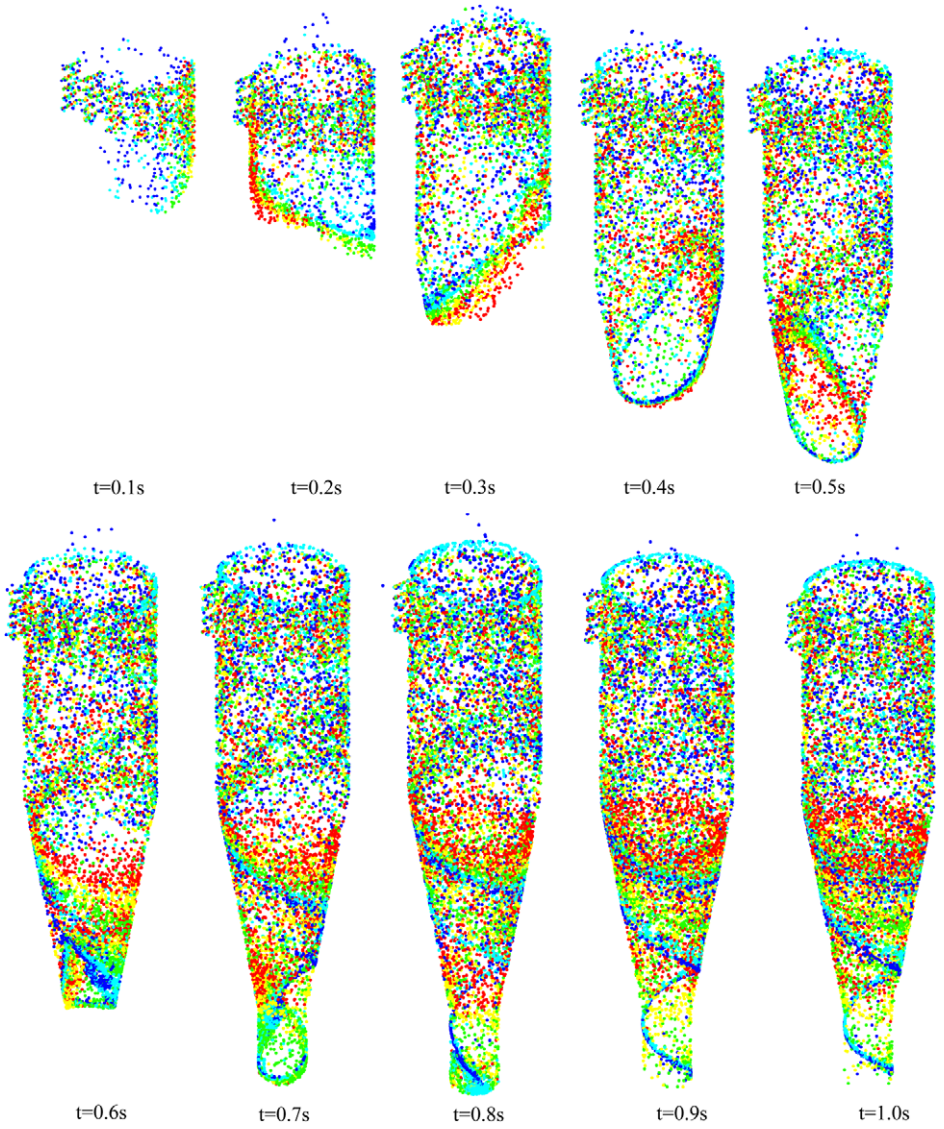

Fig. 16. Snapshots showing the flow of particles of different diameters, where red, orange, green, cyan and blue, respectively, represent five diameters of particles, which are 1×10^{-4} m, 3×10^{-5} m, 7×10^{-6} m, 2×10^{-6} m and 2×10^{-7} m (For interpretation of the references in colour in this figure legend, the reader is referred to the web version of this article).

Eq. (7) indicates that as particle diameter d_p decreases, the radius r of the orbit will decrease. If particle diameter is smaller than a critical value, and at the same time r is smaller than the radius of the hopper outlet, a particle will be collected at the bottom. When a particle is larger than this critical diameter, it will be held on the wall. There is therefore a critical value to distinguish the flow pattern of particles of different diameter. The critical value is related to the geometry of cyclone, the gas inlet velocity and the properties of particles. For the cyclone considered, the critical diameter is approximately 1×10^{-5} m.

Note that the stochastic Lagrangian model does not consider the interaction between particles. In practice, particles bigger than the critical diameter will be eventually collected at the bottom because of their interaction with other particles. Such particles, however, may also be stagnant on the wall of cyclone during the process of collection. In the cement industry, if particles at high temperatures stagnate on the wall, permanent deposition may be formed, which will seriously damage the performance of the cyclone. Moreover, this behaviour is probably responsible for the avalanche phenomenon [20].

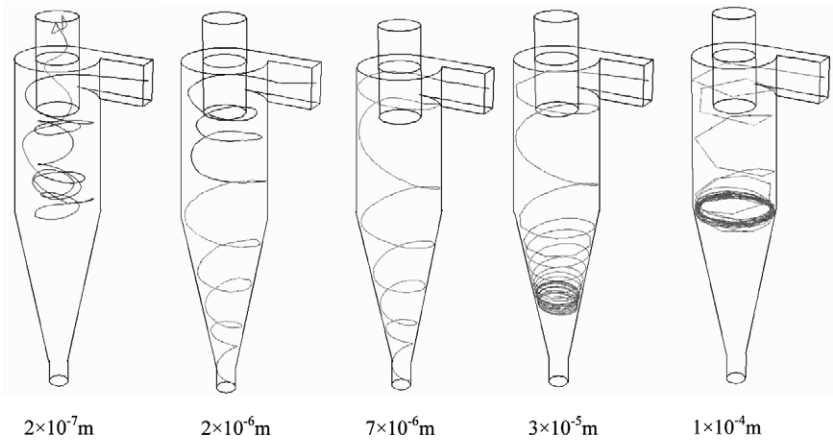

Fig. 17. The trajectories of particles with different diameters.

Fig. 18. Photos showing the trajectories of the tracing particles of different diameters (a) particles (raw material) flowing downward at the cone section and displaying a certain descending angle; (b) ceramic balls spinning at a certain height with almost zero descending angle.

4.2.3. Separation efficiency

The most important economical parameters of a cyclone separator are separation efficiency and pressure drop. Generally, the increase of gas inlet velocity will increase the separation efficiency, but it will also increase the pressure drop. In this work, physical and numerical experiments have both been done to find the effect of gas inlet velocity on separation efficiency and pressure drop. As shown in Fig. 3, the pressure drop increases with the inlet gas velocity, and there is a good agreement between the predicted and measured results. Fig. 20 shows that the collection efficiency can be enhanced with the increase of inlet gas velocity, as expected. The prediction matches the measurement reasonably well. The results further confirm the validity of the proposed model.

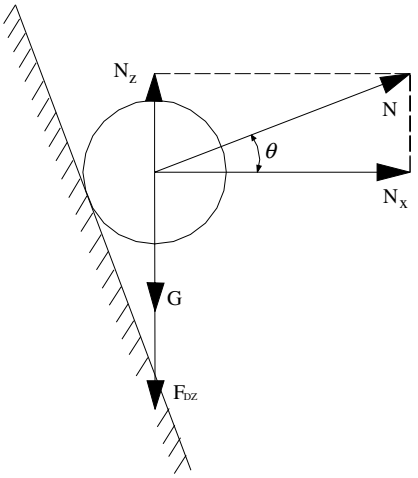

Fig. 19. Schematic diagram showing the forces on a particle in the conical part.

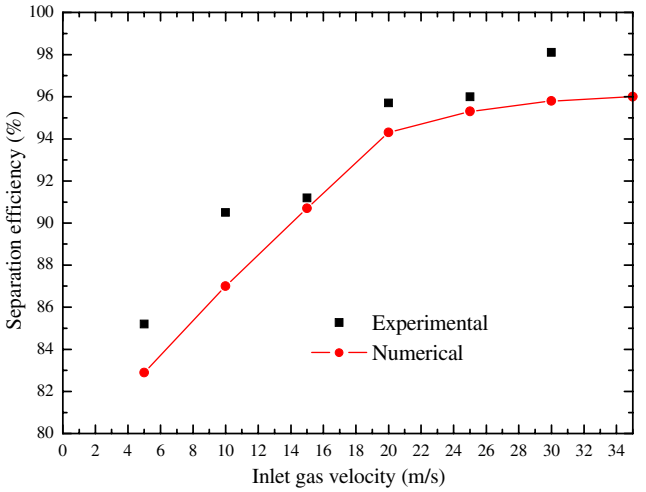

Fig. 20. Experimental vs. calculated separation efficiency.

5. Conclusions

Reynolds stress model has been used to simulate the anisotropic turbulent flow in a Lapple cyclone. Its applicability has been verified by the good agreement between the calculated and measured pressures and flow fields. On this basis, a stochastic Lagrangian model has been used to predict the flow pattern of particles in the cyclone and its validity is confirmed by comparing the predicted and measured solid flow trajectories and collection efficiency. The following conclusions can be drawn from the present study:

- The collision between gas streams after running about a circle and that just entering is the main reason for the short-circuiting flow. How to decrease the collision is probably key to designing new cyclones with high separation efficiency and low pressure drop.
- The combination of flow source and sink distributes near the axis of cyclone, resulting in a flow dipole at axial section. The orientation of the dipole is observed to locate upward along the cyclone central line. The forced vortex in the cyclone is a helical twisted cylinder.
- The secondary circulation in the cyclone is composed of short-circuiting flow, eddy flow and eccentric circumfluence. It affects the separation efficiency and pressure drop in the cyclone.

- Particles entering the cyclone at different inlet positions give different separation efficiency. Generally, particles entering from the top part of the inlet have higher separation efficiency than those from the bottom part of the inlet.
- Particles with a size exceeding a critical diameter, which may depend on cyclone geometry and flow condition, will not be collected at the cyclone bottom and may stagnate on the conical wall of the cyclone as a result of the balanced forces such as the supporting force from the wall, the gas drag force and the gravity force. This may lead to the formation of the permanent deposition on the conical part in the cyclone.

Acknowledgements

The authors are grateful to Australian Research Council (ARC) for the financial support of this work.

References

[1] F. Boysan, W.H. Ayer, J.A. Swithenbank, Fundamental mathematical-modelling approach to cyclone design, Trans. Inst. Chem. Eng. 60 (4) (1982) 222–230.
[2] A.J. Hoekstra, J.J. Derksen, H.E.A. Van Den Akker, An experimental and numerical study of turbulent swirling flow in gas cyclones, Chem. Eng. Sci. 54 (1999) 2055–2056.
[3] K. Pant, C.T. Crowe, P. Irving, On the design of miniature cyclone for the collection of bioaerosols, Powder Technol. 125 (2002) 260–265.
[4] M. Sommerfeld, C.H. Ho, Numerical calculation of particle transport in turbulent wall bounded flows, Powder Technol. 131 (2003) 1–6.
[5] E. Loth, Progr. Energy Combust. Sci. 26 (2000) 161–223.
[6] S. Yuu, N. Yasukouchi, Hirosawa, AIChE J. 24 (1978) 509–519.
[7] A.D. Gosman, E. Ioannides, Aspects of computer simulation of liquid-fuelled combustors. AIAA paper 81-0323, 1981.
[8] G.J. Sturgess, S.A. Syed, Calculation of a hollow-cone liquid spray in uniform airstream, J. Propul. Power 1 (1985) 360–369.
[9] A.A. Mostafa, H.C. Mongia, Evolution of particle-laden jet flows: a theoretical and experimental study, AIAA J. 27 (1968) 167–183.
[10] M. Sommerfeld, G. Kohnen, M. Ruger, Some open questions and inconsistencies of Lagrangian particle dispersion models, in: Proc. Ninth Symp. on Turbulent Shear Flows, Kyoto, Japan, Paper 5.1, 1993.
[11] R.J. Litchford, S.M. Jeng, Efficient statistical transport model for turbulent particle dispersion in sprays, AIAA J. 29 (1991) 1443–1451.
[12] X.Q. Chen, J.C.F. Pereira, Efficient computation of particle dispersion in turbulent flows with a stochastic-probabilistic model, Int. J. Heat Mass Transfer 40 (8) (1997) 1727–1741.
[13] R. Shun, Z.Q. Li, Simulation of strong swirling flow by use of different turbulence model, Power Eng. China 22 (3) (2002).
[14] Suasnabar, Daniel Jose, Dense medium cyclone performance enhancement via computational modelling of the physical processes, Ph.D. Thesis, University of New South Wales, 2000.
[15] J.C. Cullivan, R.A. Williams, T. Dyakowski, C.R. Cross, New understanding of a hydrocyclone flow field and separation mechanism from computational fluid dynamics, Miner. Eng. 17 (2004) 651–660.
[16] S.V. Alekseenko, P.A. Kuibin, V.L. Okulov, S.I. Shtork, Helical vortices in swirl flow, J. Fluid Mech. 382 (1999) 195–243.
[17] A.J. Hoekstra, Gas flow field and collection efficiency of cyclone separators, Ph.D. Thesis, Delft University of Technology, 2000.
[18] St. Schmidt, H.M. Blackburn, M. Rudman, Impact of outlet boundary conditions on the flow properties within a cyclone, 15th Australasian Fluid Mechanics Conference, The University of Sydney, Sydney, Australia, 13–17 December 2004.
[19] D. Bradley, The Hydrocyclone, Pergamon, London, 1965.
[20] H.F. Meier, K. Ropelato, M. Mori, et al., Computational fluid dynamics CFD for cyclone evaluation and design, ZKG Int. 55 (6) (2002) 58–64.